ELSEVIER

NeuroImage

www.elsevier.com/locate/ynimg
NeuroImage 39 (2008) 348–358

Assessment of brain growth in early childhood using deformation-based morphometry

P. Aljabar,[a,*] K.K. Bhatia,[a] M. Murgasova,[a] J.V. Hajnal,[c] J.P. Boardman,[b,c] L. Srinivasan,[b,c] M.A. Rutherford,[c] L.E. Dyet,[b] A.D. Edwards,[b,c] and D. Rueckert[a]

[a]*Visual Information Processing Group, Department of Computing, Imperial College London, London, UK*
[b]*Department of Paediatrics, Imperial College, Hammersmith Hospital, London, UK*
[c]*MRC Clinical Sciences Centre, Imperial College, Hammersmith Hospital, London, UK*

Received 8 February 2007; revised 17 July 2007; accepted 30 July 2007
Available online 24 August 2007

We present methods for the quantitative analysis of brain growth based on the registration of longitudinal MR image data with the use of Jacobian determinant maps to characterise neuroanatomical changes. The individual anatomies, growth maps and tissue classes are also spatially normalised in an 'average space' and aggregated to provide atlases for the population at each timepoint. The average space representation is obtained using the average intersubject transformation within each timepoint. In an exemplar study, this approach is used to assess brain development in 25 infants between 1 and 2 years, and we show consistency in growth estimates between registration and segmentation approaches.

Keywords: Registration; Atlases; Growth

Introduction

Most previous neuroinformatic studies of human brain growth have focused on older children and adolescents (Huppi et al., 1998; Nishida et al., 2006; Giedd et al., 1996; Matsuzawa et al., 2001). However, the majority of brain growth occurs during the first two years of life, much occurring in utero prior to birth at 40 weeks' gestational age, and a full understanding of human brain development must include this early period of rapid development. Many previous studies have used cross-sectional designs, in which intersubject variability can add an additional confound, and longitudinal data are likely to be more accurate. Growth studies based on longitudinal data include tissue growth models (Giedd et al., 1999) for ages 4 to 20, development tracking of particular structures in a group of six children (3–15 years) (Thompson et al., 2000) and atlas-based regional growth estimates for eight subjects scanned at 2 and 4 years (Gerig et al., 2006). Some approaches have been nonvolumetric, for example the cortical thickness measurements (5–11years) presented in Sowell et al. (2004). A critical review of literature relating to MRI studies of the developing brain can be found in Durston et al. (2001). Longitudinal studies in the very immature brain have been challenging for existing neuroinformatic approaches, and we now present a new method suitable for longitudinal studies in infants and very young children.

In earlier work (Boardman et al. (2006, 2005a,b)), we used maps of the Jacobian determinant to identify volumetric group differences between preterm born children and term born controls. This approach, where derivatives of the deformation field are used to characterise regional differences, is sometimes described as Deformation-Based Morphometry (DBM) (Davatzikos et al., 1996; Chung et al., 2001), and contrasts with Voxel-Based Morphometry (VBM) (Ashburner and Friston, 2000) where, after images have been spatially normalised, the main focus of study are the differences in tissue properties at individual voxels. The DBM approach has particular attractions for studies of the immature brain where rapid changes in voxel properties create challenges for VBM. We have previously shown that growth estimates for children between 1 and 2 years of age can be consistently derived using DBM applied either to the individual baseline and follow-up scans or to average space atlases representing the cohort at each timepoint (Aljabar et al., 2006).

In this study, we provide estimates for global and regional growth in an exemplar group of 25 infants who were born preterm, and from whom volumetric magnetic resonance(MR) imaging data were acquired at both one and two years of age. There is a particular need to characterise and quantify brain development in this vulnerable population: extreme preterm delivery potentially disrupts brain growth and many children born prior to 26 weeks' gestational age develop neurological disabilities (Marlow et al., 2005) and neurocognitive problems that can continue into

* Corresponding author.
E-mail address: paul.aljabar@imperial.ac.uk (P. Aljabar).
Available online on ScienceDirect (www.sciencedirect.com).

1053-8119/$ - see front matter © 2007 Elsevier Inc. All rights reserved.
doi:10.1016/j.neuroimage.2007.07.067

adolescence (Botting, 1997). We also present average space atlases of the anatomy at each timepoint and average space maps of regional growth. Growth estimates from individual registrations and from atlas-based estimates are compared and shown to be consistent with estimates obtained from conventional tissue segmentation.

In the next section, we describe the data that we used and how they were preprocessed, registered and used to obtain growth estimates and generate atlases of different aspects of the population (e.g. anatomy or growth). The results of the registrations and growth estimates are shown in the following section along with atlases of the population in average space for anatomy, growth and tissue class. Also included are tissue volumes at each timepoint for white and grey matter along with a comparison of growth estimates across the group provided by registration and segmentation. We present a discussion of our results in the final section.

Materials and methods

The subjects for this study are 25 preterm born children (9 female, 16 male) who were scanned at one and two years of age. The mean gestational age at birth was 27.7 weeks (SD 2.2), the mean corrected ages at scan were 54.0 weeks (SD 5.8) for the 1 year (baseline) scans and 106.4 weeks (SD 4.4) for the 2 year (follow-up) scans. Scan ages corrected for gestational age by recording the ages of the children relative to their due dates at 40 weeks gestation rather than the actual premature birth dates. The mean interval between corresponding scans was 52.4 weeks (SD 7.1). Ethical permission was obtained to sedate the children during scanning as this increases the likelihood of a successful acquisition.

The scans acquired for all children wereT1 weighted MR volumes. Seven subjects' images were acquired using a Marconi 0.5 T Apollo scanner, TR/TE=23 ms/6 ms, flip angle=30°. The images for the remaining subjects were acquired using 1.0 T HPQ system (Philips Medical Systems, Cleveland, Ohio), TR/TE=23 ms/6 ms, flip angle=35°. All images were reconstructed with voxel dimensions of $1\times1\times1.6$ mm^3. The images were preprocessed initially by correcting for MR nonuniformity. This was achieved using 'N3' (Sled et al., 1998). Brain masks were created for the images using 'BET' (Smith, 2002). These assist the registration and tissue segmentation steps by defining a region of interest.

Our aim is to use these data to quantify growth for individual subjects during the second year of life. Registration-based growth estimates are calculated over the whole brain and are also transformed to a common coordinate system and aggregated to produce a population average. Quantifying brain development for young children poses a considerable challenge due to factors such as scale of the developmental changes involved and the variations in intensity response (e.g. due to myelination). We have validated our growth estimates by comparing them with estimates provided by a tissue segmentation algorithm.

In order to obtain registration-based growth estimates, for individuals or for the cohort, two types of registration were carried out. A longitudinal registration was performed for each subject using the baseline and follow-up scans. The transformations obtained from longitudinal registration can be used to provide estimates of growth for each subject by calculating the Jacobian determinant. We also carried out cross-sectional registrations within each timepoint by randomly selecting a reference subject and registering the remaining subjects within the timepoint to the reference. The cross-sectional transformations allow us to generate atlases at each time-point in the space of the reference subject. By using the average cross-sectional transformation to the reference, however, we were able to generate 'average space' atlases within each time-point. These atlases can represent anatomy, particular structures or regional growth for the population. A schematic diagram for the different registrations and the atlases is illustrated in Fig. 1.

The methods used to register images and for estimating growth are described in the next section. Details of the atlas construction, averaging transformations and aggregating growth estimates are then presented. This is followed by a description of the tissue segmentation method.

Registration and growth estimation

Registration

For a given pair of images, registration was carried out in two steps. A global transformation was first estimated using a 12 parameter affine registration. An affine registration was chosen for the initial step (as opposed to a rigid transformation) because global shape changes due to growth take place during early childhood. Subsequently, using the result of the affine registration as a starting point, a non-rigid registration step was carried out. To clarify terminology, we describe one image as the 'target' and the second image as the 'source'. After registration, the obtained transformation maps locations in the target to locations in the source.

Let $\mathbf{T}_{\text{global}}$ represent a global affine transformation and $\mathbf{T}_{\text{local}}$ a local non-rigid displacement field. The global transformation can be represented by a translation vector $\mathbf{d}$ and a 9 parameter affine matrix $\mathbf{M}$ encoding rotations, scales and shears: $\mathbf{T}_{\text{global}}(\mathbf{x})=\mathbf{M}\mathbf{x}+\mathbf{d}$. The complete transformation $\mathbf{T}$ that accounts for both

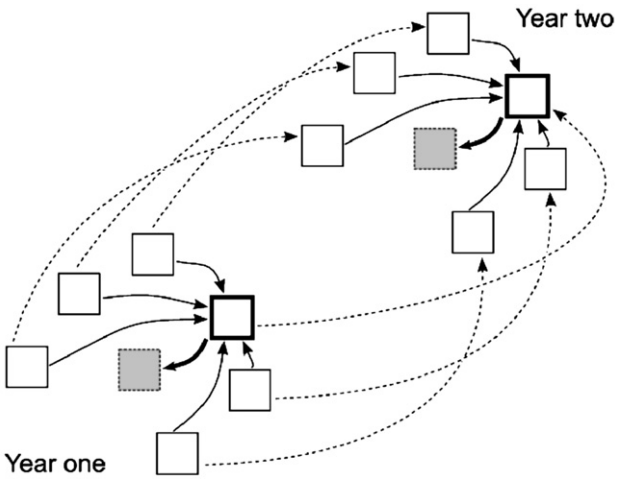

Fig. 1. Schematic illustration of the images used and registrations performed. The subject images are represented by the clear squares with the reference subject shown in bold. The year 1 (baseline) and year 2 (follow-up) images for each subject are registered to obtain longitudinal transformations (shown as dashed arrows). Within each timepoint, the subjects are registered to the reference (solid arrows) and the average transformation (bold arrows) is used to map reference locations to the average space (grey square). Atlases were generated in the average space which could represent anatomy, growth or tissue class across the population.

global and local differences between a pair of images is modelled as the sum of these local and global components

$$\mathbf{T}(\mathbf{x}) = \mathbf{T}_{\text{global}}(\mathbf{x}) + \mathbf{T}_{\text{local}}(\mathbf{x}) = \mathbf{M}\mathbf{x} + \mathbf{d} + \mathbf{T}_{\text{local}}(\mathbf{x}) \quad (1)$$

for each location $\mathbf{x}$ in the target image.

The non-rigid deformations were represented using the free-form deformation (FFD) model (Sederberg and Parry, 1986; Rueckert et al., 1999). A free-form deformation can be parametrised by a set of vectors $\{\mathbf{\Phi}_{i,j,k}\}$ associated with a regular $n_x \times n_y \times n_z$ lattice of control points with spacings of δ_x, δ_y and δ_z along each dimension. The local displacement at a location (x,y,z) is given by a B-spline tensor product over the control point vectors

$$\mathbf{T}_{\text{local}}(x,y,z) = \sum_{l=0}^{3}\sum_{m=0}^{3}\sum_{n=0}^{3} B_l(r)B_m(s)B_n(t)\mathbf{\Phi}_{i+l,j+m,k+n}$$

where $i=\lfloor x/\delta_x \rfloor - 1$, $j=\lfloor y/\delta_y \rfloor - 1$ and $k=\lfloor z/\delta_z \rfloor - 1$, $r=x/\delta x - i$, $s=y/\delta_y - j$ and $t=z/\delta_z - k$. B_0, …, B_3 are the cubic B-spline basis functions. During each of the affine and non-rigid registration steps, the cost function C that was optimised was represented by the sum of a similarity metric $C_{\text{similarity}}$ and a weighted smoothness penalty C_{smooth},

$$C = C_{\text{similarity}} + \lambda C_{\text{smooth}}.$$

The similarity metric used was normalised mutual information (NMI) (Studholme et al., 1998) and the smoothness penalty was represented by the bending energy associated with the transformation (Wahba, 1990; Rueckert et al., 1999). The value of λ used in the cost function was set empirically to 0.01. The transformation parameters were optimised using gradient ascent.

The non-rigid registration was carried out in a coarse-to-fine manner (Schnabel et al., 2001) with successive control point spacings of 20 mm, 10 mm, 5 mm and 2.5 mm. The initial spacing represents the larger scale non-rigid deformations with the subsequent spacings used to capture increasingly finer detail. The FFD resulting from optimising each control point spacing is used as an initial estimate for the next.

Growth estimation

To characterise growth in individual subjects, we carried out intra-subject registrations using the baseline and follow-up scans as target and source images respectively. For a given pair of images and a transformation $\mathbf{T}=(T_x, T_y, T_z)$ mapping target to source locations, the Jacobian operator D can be applied to the transformation,

$$D\mathbf{T} = \begin{pmatrix} \frac{\partial T_x}{\partial x} & \frac{\partial T_x}{\partial y} & \frac{\partial T_x}{\partial z} \\ \frac{\partial T_y}{\partial x} & \frac{\partial T_y}{\partial y} & \frac{\partial T_y}{\partial z} \\ \frac{\partial T_z}{\partial x} & \frac{\partial T_z}{\partial y} & \frac{\partial T_z}{\partial z} \end{pmatrix}$$

and the volume change induced by the transformation at a target location $\mathbf{x}$ is given by the determinant of the Jacobian at $\mathbf{x}$ which can be denoted $J(\mathbf{x})$. From Eq. (1),

$$J(\mathbf{x}) = \det(D\mathbf{T}(\mathbf{x}))$$

$$= \det(D\mathbf{T}_{\text{global}}(\mathbf{x}) + D\mathbf{T}_{\text{local}}(\mathbf{x}))$$

$D\mathbf{T}_{\text{global}}(\mathbf{x})=\mathbf{M}$ and $D\mathbf{T}_{\text{local}}(\mathbf{x})$ can be calculated analytically using the derivatives of the B-spline basis functions.

The Jacobian determinant can be used to estimate growth over particular tissue classes. If Ω represents a tissue class(e.g. white matter) within a baseline image, then the degree of membership of a voxel within Ω can be modelled as a spatially varying probability map $p(\mathbf{v})$, where $0 \le p(\mathbf{v}) \le 1$ for voxels $\mathbf{v}$ in the image domain V. The tissue volumes were calculated by summation of the tissue probability maps over the domain, i.e. $|\Omega| = \sum_{\mathbf{v}\in V} p(\mathbf{v})$. The growth factor for the tissue class can be estimated using the expression

$$\frac{|\mathbf{T}(\Omega)|}{|\Omega|} \approx \frac{\sum_{\mathbf{v}\in V} p(\mathbf{v})J(\mathbf{v})}{\sum_{\mathbf{v}\in V} p(\mathbf{v})}. \quad (2)$$

Atlas construction and transformation averaging

Atlas construction

To characterise population growth or to estimate region-specific growth patterns and to help visualise typical anatomies, atlases were created to represent the cohort at each time-point based on intersubject registrations between the cohort and a reference within the same timepoint.

In order to avoid dependence on or bias towards any particular subject, i.e. the chosen reference, these atlases were created in an 'average space'. A number of approaches have been used to generate average space (or 'template free') atlases (Bhatia et al., 2004, 2005; Lorenzen et al., 2004, 2005; Avants and Gee, 2004; Rueckert et al., 2003; Craene et al., 2004) and our approach is based on estimating the average intersubject transformation within each timepoint (Aljabar et al., 2006). We now describe the method of atlas construction and follow this with details of the methods used to average transformations.

Anatomical atlases for the subjects were created for the images with in a timepoint based on the intersubject transformations for that timepoint. The intersubject registrations all use a reference subject as the target image but the possible bias towards the reference was reduced using the average of intersubject transformations. This process is schematically illustrated in Fig. 2.

Let $\{I_1, \ldots, I_n\}$ represent the images for all subjects within a timepoint and I_{ref} represent the reference subject's image. Let $\{\mathbf{T}_1, \ldots, \mathbf{T}_n\}$ denote the intersubject transformations (with I_{ref} as target) and let the result of averaging these transformations be denoted $\mathbf{T}_{\text{av}}$. As with the input transformations, I_{ref} is the target image for $\mathbf{T}_{\text{av}}$; however, it will map locations in I_{ref} to a

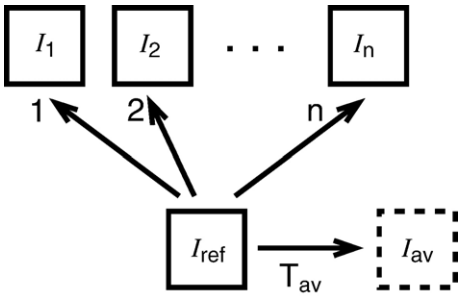

Fig. 2. Atlas construction within a timepoint. The numbered arrows show the transformations between the reference and the remaining subjects. These transformations are averaged to create $\mathbf{T}_{\text{av}}$. The compositions of $\mathbf{T}_{\text{av}}^{-1}$ and the individual transformations were used to create an atlas in the average space.

postulated average space image I_{av}. The composition of $\mathbf{T}_{av}^{-1}$ with each of $\{\mathbf{T}_1, \ldots, \mathbf{T}_n\}$ can be used to map locations in I_{av} to each of the individual subjects' images. This method is similar to the approach used by Guimond et al. (2000) and Rueckert et al. (2003) for averaging local deformations. Our approach differs in that we retain the global affine component of the transformations during averaging.

The inversion of the global affine component of $\mathbf{T}_{av}$ is straightforward but the local FFD component is not analytically invertible. We used a numeric method to invert the FFD by starting a lattice of control points in the space of the reference image (which has the same position and orientation as the average space atlas). For each control point location (x,y,z) an estimate of the displacement $\mathbf{T}_{av}^{-1}(x,y,z)$ was obtained using a Newton method. Once all the displacements are obtained for the control point locations, a set of B-spline FFD components are calculated for each control point using the inverse filtering method described by Unser (1999).

The images used during intersubject registration were the anatomical MR images whereas the data used to create subsequent atlases can be drawn from multiple sources. Atlas images can be created for anatomies, individual growth maps (based on longitudinal transformations) or tissue probability maps.

If the images to be averaged are anatomies (after alignment in the common coordinate system) then the intensities within each image are first converted to z-scores by subtracting the image mean and dividing by the standard deviation. The z-scores are in turn linearly averaged across all the images to produce an average value at each voxel. The values in this image are then linearly shifted and scaled to have a fixed chosen mean and standard deviation. If the images to be averaged are tissue probability maps, then they are already normalised to the same range and are linearly averaged. If the atlased images represent growth maps for each subject, $\{J_1, \ldots, J_n\}$, then their values at a corresponding voxel $\mathbf{v}$ (in the common coordinate system) are combined using their geometric mean

$$J_{av}(\mathbf{v}) = \left(\prod_{i=1}^{n} J_i(\mathbf{v})\right)^{\frac{1}{n}} \tag{3}$$

The geometric mean was chosen for averaging the Jacobian determinant values as they were treated as multiplicative scale factors for the volume of each voxel. The values used for $J_i(\mathbf{v})$ are obtained by normalising Jacobian determinant values calculated from the longitudinal transformation according to the interval between scans. This was done to account for the variability in the intervals between scans. The normalisation was carried out geometrically again, i.e. for an interscan interval of d days and a calculated Jacobian determinant value of $\mathcal{J}_i(\mathbf{v})$ for the ith subject at voxel $\mathbf{v}$, the determinant value used, $J_i(\mathbf{v})$, was given by

$$J_i(\mathbf{v}) = (\mathcal{J}_i(\mathbf{v}))^{\frac{365}{d}}$$

Averaging transformations

As described earlier, the average intersubject transformation to a reference subject was used during the creation of average space atlases. This is carried out separately for the global and local parts of the transformations with the results subsequently combined.

Averaging global transformations

The average global transformation was estimated for the subjects within a timepoint separately from the non-rigid deformation fields. Using the same notation as that used above, we have a set of transformations $\{\mathbf{T}_1, \ldots, \mathbf{T}_n\}$ relating each subject to the reference. For a given i, $\mathbf{T}_i$ is represented by

$$\mathbf{T}_i(\mathbf{x}) = \mathbf{T}_{global,i}(\mathbf{x}) + \mathbf{T}_{local,i}(\mathbf{x}) = \mathbf{M}_i\mathbf{x} + \mathbf{d}_i + \mathbf{T}_{local,i}(\mathbf{x}) \tag{4}$$

i.e. the global transformation is determined by affine matrix $\mathbf{M}_i$ and translation $\mathbf{d}_i$. $\mathbf{M}_i$ can be decomposed as $\mathbf{M}_i = \mathbf{R}_i\mathbf{A}_i$ where $\mathbf{R}_i$ is a rotation matrix and $\mathbf{A}_i$ represents scales and shears.

If the full set of global parameters $\{\mathbf{M}_i, \mathbf{d}_i\}_{i=1\ldots n}$ is used in the averaging process, then the resulting atlas will also reflect the average position and orientation of the images (relative to the reference).This position and orientation information are independent of the anatomical and growth data we seek to characterise so only the matrices $\{\mathbf{A}_i\}_{i=1\ldots n}$ were used in the averaging process, providing an estimate of the average with respect to global size and shape.

Algorithm 1. Find the Frechét mean of a set of matrices.

Input: Matrices $\{\mathbf{A}_i\}_{i=1..n}$
Output: Frechét mean $\mathbf{A}_{av}$
$\mathbf{A}_{av} = \mathbf{I}$
do
$\mathbf{A}' = \exp\left\{\frac{1}{n}\sum_{i=1}^{n}\log\left(\mathbf{A}_{av}^{-1}\mathbf{A}_i\right)\right\}$
$\mathbf{A}_{av} = \mathbf{A}_{av}\,\mathbf{A}'$
while ($\|\log(\mathbf{A}')\| > \epsilon$)

The average $\mathbf{A}_{av}$ of the matrices $\{\mathbf{A}_i\}$ is given by their Frechét (or intrinsic) mean and is calculated using Algorithm 1. In this algorithm, the log operation maps matrices from their (nonlinear) manifold to the tangent space where they are linearly averaged and subsequently mapped back from the tangent space to the manifold using the exponential map. This approach to averaging elements of nonlinear spaces has previously been used for averaging transformations (Bossa and Olmos, 2006; Alexa, 2002) and for averaging tensor data (Arsigny et al., 2005).

Averaging local deformations

As shown in Eq. (4), the individual transformations are expressed as the sum of a global transformation and a local FFD displacement field $\mathbf{T}_{local,i}$. In order to remove the effect of the global transformation before averaging, the local components of the individual transformations, the control point vectors $\{\Phi_{u,v,w}\}_i$ for each local displacement field $\mathbf{T}_{local,i}$ are premultiplied by the Jacobian of the inverse affine transformation (Rueckert et al., 2003; Rao et al., 2006) to obtain

$$\{\Phi'_{u,v,w}\}_i = \{\mathbf{M}_i^{-1}\Phi_{u,v,w}\}_i$$

The control points $\{\Phi'_{u,v,w}\}_i$ are linearly averaged over $i = 1\ldots n$ to produce $\{\Phi_{u,v,w'}\}_{av}$ which are then coupled with the average global transformation $\mathbf{A}_{av}$ to generate the control points of the local component, $\mathbf{T}_{local,av}$, of the complete average transformation as follows

$$\{\Phi_{u,v,w}\}_{av} = \{\mathbf{A}_{av}\Phi'_{u,v,w}\}_{av}$$

With the average affine matrix and average local deformation field calculated, the average complete transformation $\mathbf{T}_{av}$ of the input transformations $\{\mathbf{T}_1, \ldots, \mathbf{T}_n\}$ is then expressed as the sum

$$\mathbf{T}_{av}(\mathbf{x}) = \mathbf{A}_{av}\mathbf{x} + \mathbf{T}_{local,av}(\mathbf{x})$$

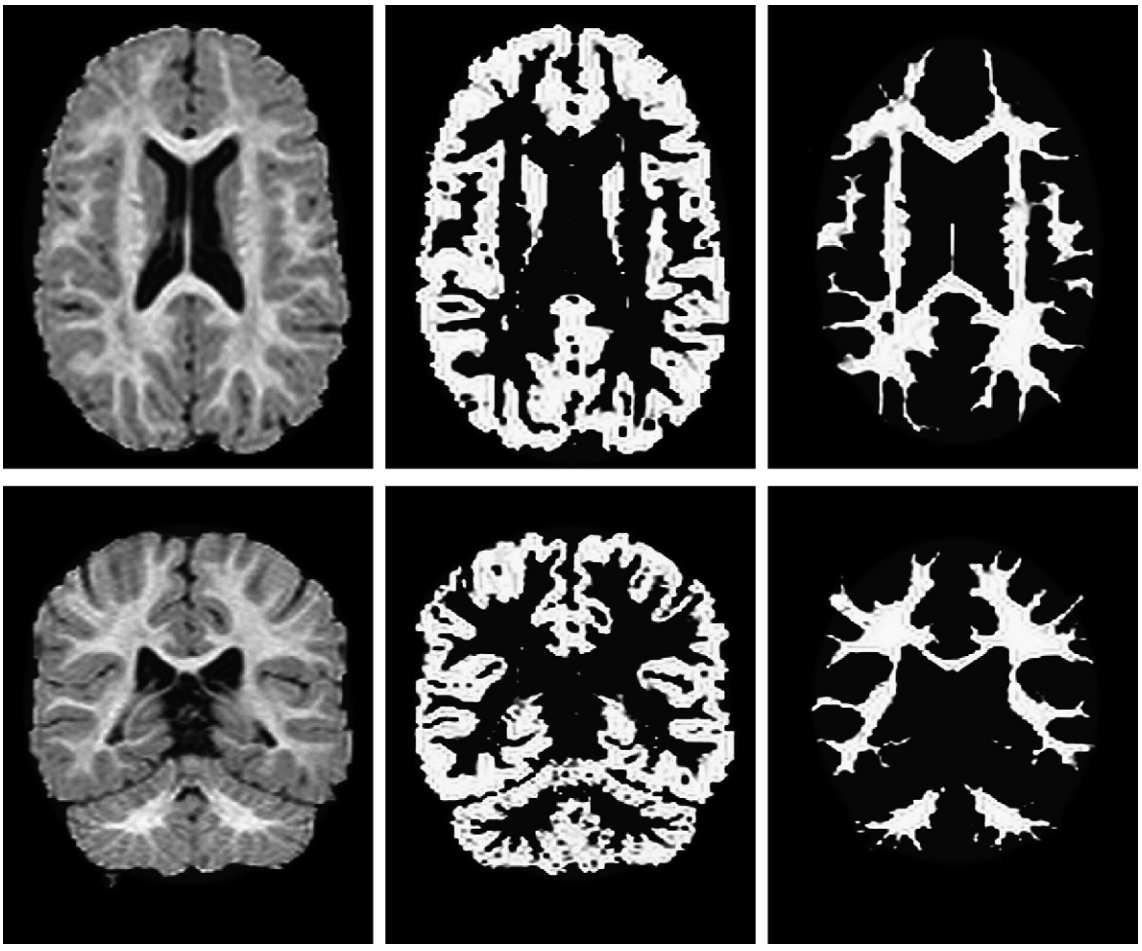

Fig. 3. Segmentations for grey and white matter produced by the tissue segmentation algorithm for an individual subject.

Image segmentation

In order to provide alternative growth estimates for validation, a method based on expectation maximisation (EM) (Leemput et al., 1999) and the use of atlases of prior tissue membership probabilities was used to provide tissue probability maps for each subject. While EM-based methods have a proven track record in classifying the tissues of adult brain images, the specific tissue

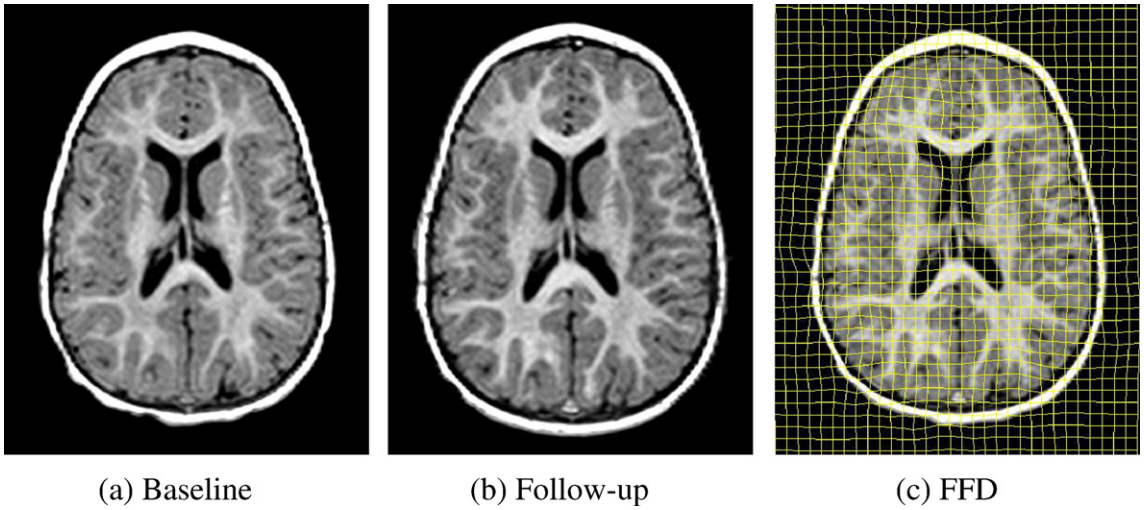

Fig. 4. The left and middle images show the baseline (year 1) and follow-up (year 2) images for a particular subject. The right image shows the follow-up image after non-rigid registration along with the grid used for the free form deformation.

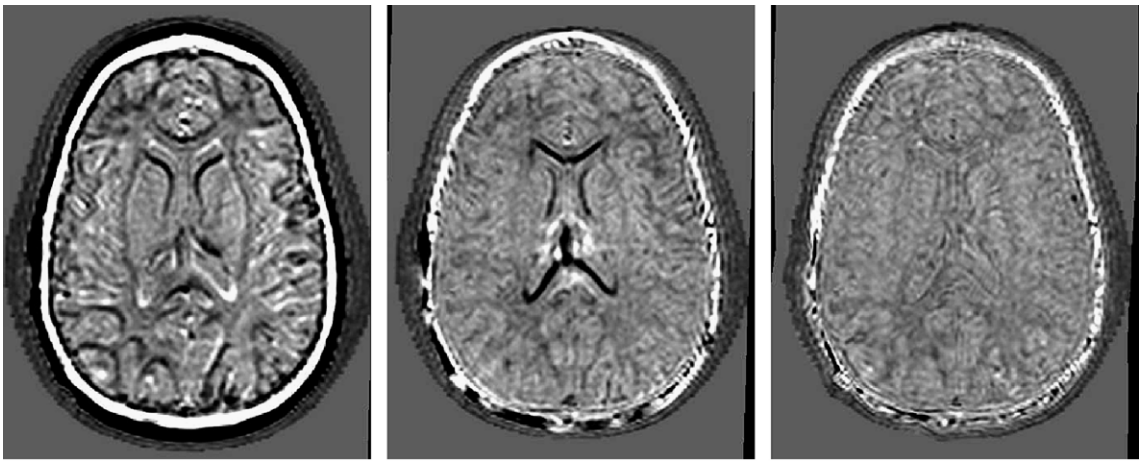

Fig. 5. Difference images between the baseline and follow-up images after a rigid alignment and after the affine and non-rigid registration steps. These images are of the same subject shown in Fig. 4, i.e. panel a shows the difference between Figs. 4a and b.

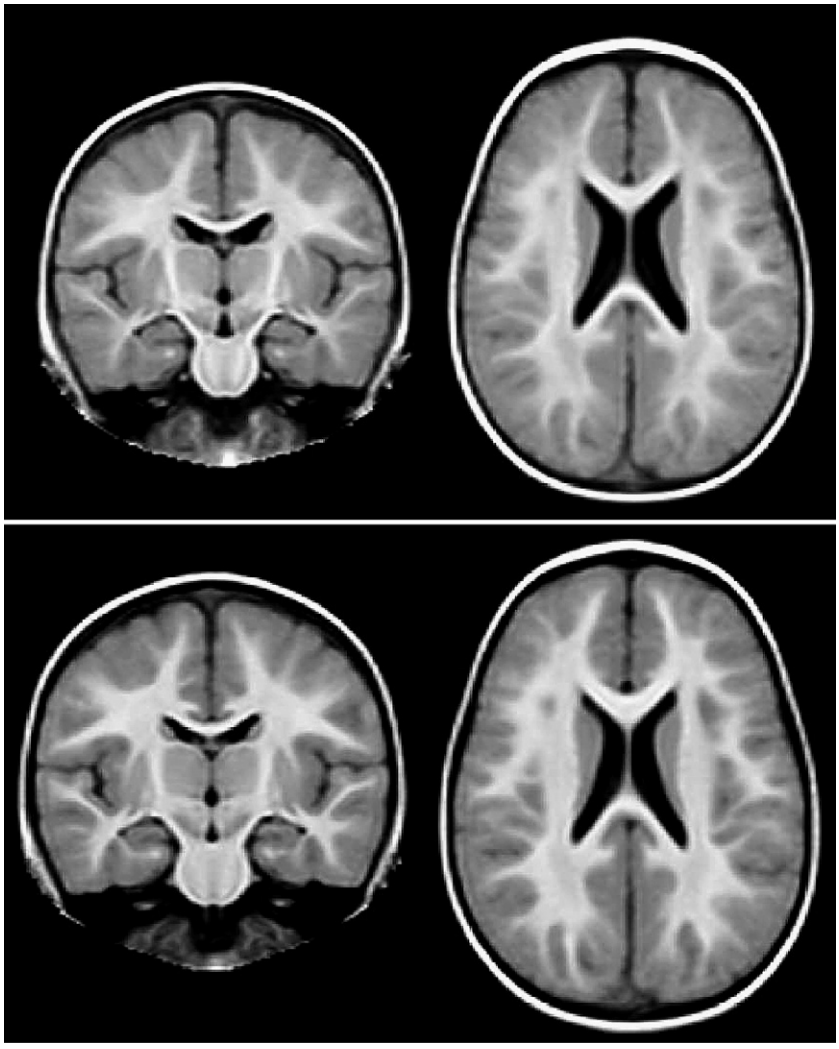

Fig. 6. The average space anatomical atlases of the cohort based on the one year scans (top) and the two year scans (bottom).

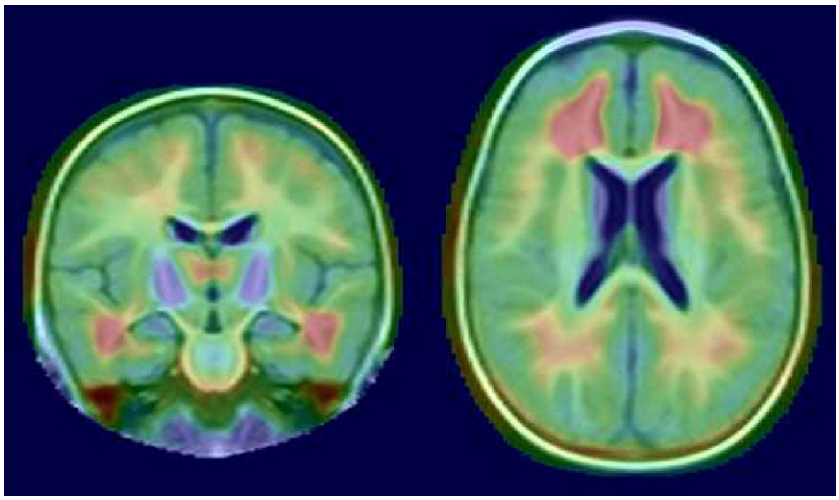

Fig. 7. The growth map atlas based on all individual growth maps. This is in the space of the year 1 (baseline) average space atlas.

properties in the images of children, however, present a significant challenge. We were able to obtain improved segmentations by creating probabilistic atlases at each time-point based on manual segmentations of a single subject. These were, in turn, transformed to the space of each subject before being used as prior probability maps (Murgasova et al., 2006). Examples of the segmentations produced by the EM algorithm are shown in Fig. 3.

Results

Individual registration results

The baseline and follow-up images for an individual are shown in Fig. 4 along with an illustration of the transformed follow-up image after non-rigid registration, this also shows the deformed lattice of control points used to transform the image.

Images showing the difference between the baseline and follow-up images are shown in Fig. 5. Fig. 5(a) shows the difference image after a rigid alignment. Figs. 5(b) and (c) show the difference image after affine and non-rigid registration respectively.

The effect of the choice of regularisation parameter was evaluated by finding the percentage of voxels with a negative Jacobian determinant for each of the various transformations. For the longitudinal transformations, between the baseline and follow-up images, two of the 25 subjects' transformations contained negative determinants and these occurred in less than 10^{-3}% of the voxels. For the cross-sectional transformations used to create the atlases, the average percentage of voxels with negative Jacobian determinants was 0.03% (SD 0.06%, maximum 0.3%). The average transformations used to create the average space atlases did not generate any negative Jacobian determinant values.

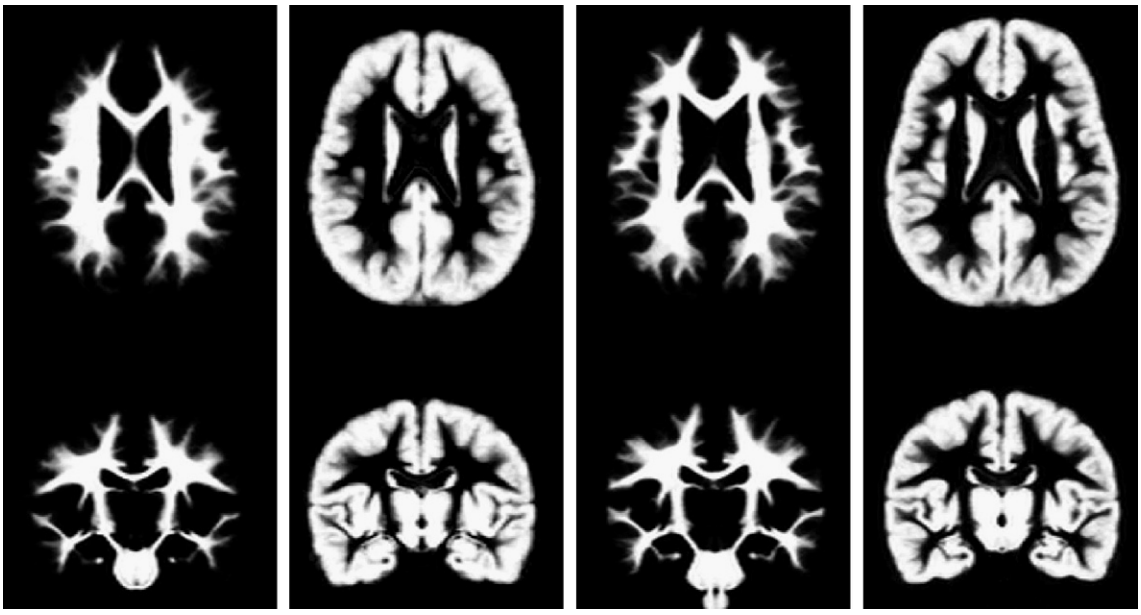

Fig. 8. The average space atlases of the tissue maps. From left to right: WM year 1, GM year 1, WM year 2, GM year 2.

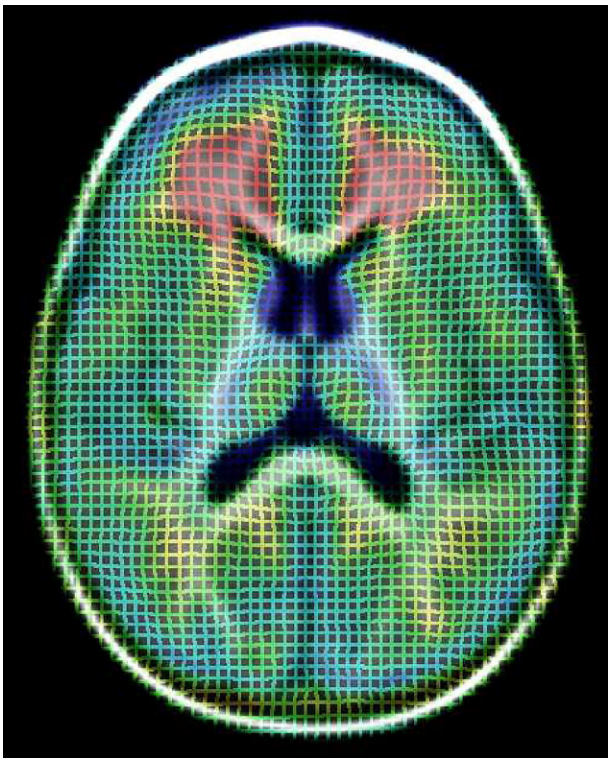

Fig. 9. An illustration of the average longitudinal deformation across the cohort. The individual longitudinal transformations were mapped to the space of the anatomical 1 year atlas and linearly averaged.

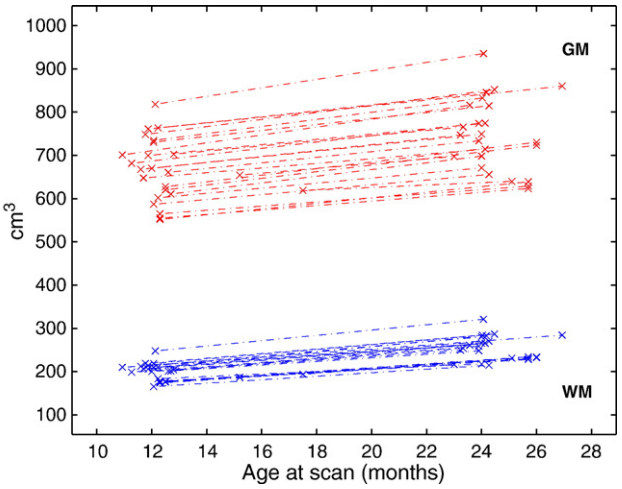

Fig. 11. Tissue volumes at ages 1 and 2 based on the segmentation results. The baseline and follow-up volumes of each tissue for an individual are joined with a dashed line to show the correspondences.

Atlases

Using the methods described above, we obtained average space atlases of anatomy at each time-point, these are illustrated in Fig. 6. Similarly, in the same coordinate system, an atlas of growth as measured by Jacobian determinants is shown in Fig. 7. Atlases of the tissue maps across the population at each timepoint are shown in Fig. 8.

In order to obtain an estimate of the average deformation that is produced by the registration of the year one and year two images, the individual longitudinal registrations for all the subjects were transformed to the space of the year one average space atlas. The method used to map the individual deformation fields to the atlas is described in Rao et al. (2004). After spatial alignment of the deformation fields, their control points were averaged to produce the average deformation field as described earlier. An illustration of the average deformation is shown in Fig. 9 where the deformations have been enlarged by 50% in order to give a sense of the patterns of change across the group.

In order to assess the influence of the choice of reference subject used during the construction of the average space atlas, two

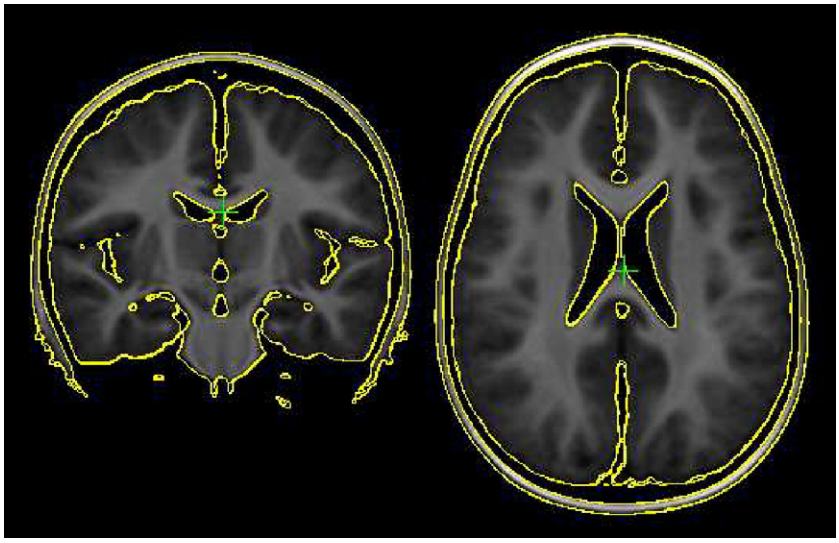

Fig. 10. Two corresponding iso-intensity contours taken from each of a pair of average space atlases. The atlases were generated using two different reference subjects, i.e. two different choices for the subject labelled I_{ref} in Fig. 2. The atlases were rigidly aligned using the rigid transformation relating the corresponding reference subjects.

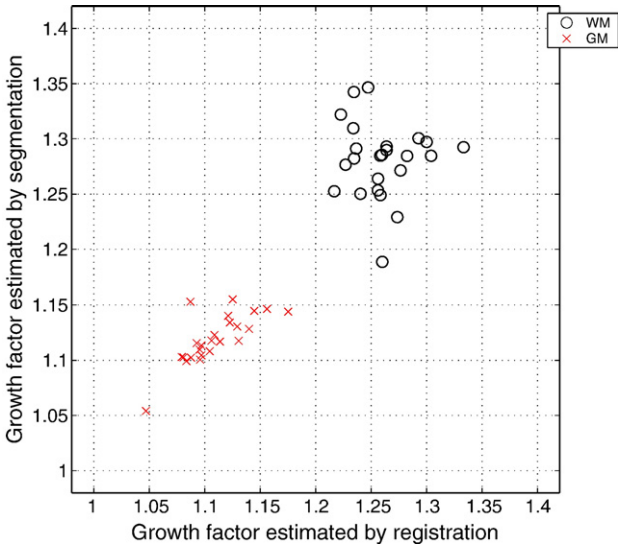

Fig. 12. GM and WM growth factor estimates for all subjects. This chart shows the general agreement between estimates of growth provided by registration and those provided by segmentation. The registration-based figures are derived using Eq. (2) and the segmentation-based figures are the ratio of the volumes of each tissue at the two timepoints.

average space anatomical atlases were generated using two different reference subjects. Each atlas has the same orientation as its corresponding reference (with respect to translation and rotation parameters) so a rigid transformation was used to align the atlases Fig. 10 shows two sets of iso-intensity contours that correspond to the same intensity taken from each of the atlases after rigid alignment.

Comparison of registration- and segmentation-based growth estimates

The tissue segmentations can be used to provide individual tissue volumes for grey and white matter for each subject at each timepoint. These are plotted in Fig. 11. In this figure, the baseline and follow-up volume estimates for a particular tissue that correspond to the same subject are joined with a dashed line. This is simply to show corresponding volumes and not intended to suggest that the growth is linear. The mean volumes of grey matter for the cohort were 665.7 (69.7) cm^3 at age one and 746.7 (81.9) cm^3 at age two, where the figures in brackets indicate standard deviations. The corresponding volumes of white matter at ages one and two were 198.7 (18.6) cm^3 and 254.8 (26.7) cm^3.

The segmentation algorithm provides maps for grey matter, white matter and cerebro-spinal fluid. Since our interest is in quantifying tissue growth, we have only used the grey and white matter maps to generate growth figures. Using the segmentation results, the growth factor for a tissue class for an individual can be estimated by finding the ratio of the volumes given by the tissue segmentation algorithm within the baseline and follow-up images. Alternatively, using the registration results, the growth factor for a tissue can be estimated using the Jacobian determinant map and the baseline tissue segmentation (see Eq. (2)).

For validation purposes, the growth factors estimated by registration for each tissue class were compared against the growth factors obtained from segmentation. This comparison between growth factors provided by registration and segmentation is illustrated in Fig. 12 and shows good agreement between the two methods. Table 1 gives a summary of the growth factors obtained by both methods for grey and white matter.

By using the average space tissue maps for grey and white matter (Fig. 8) and the average space growth map atlas (Fig. 7), a single population estimate for the growth of each tissue class was also obtained, again by integration. These whole population estimates for the growth of each tissue based on the use of atlases are shown in Fig. 13. In this figure, a separate plot is given for each tissue type and the individual growth factor estimates are also plotted for comparison.

Discussion

We have shown in this work how the current techniques of DBM and the registration of longitudinal data can be used to generate quantitative estimates of brain growth for a cohort and for individual subjects during the second year of life. We have applied these techniques to images of preterm born children. Data for term born controls are relatively scarce (as we do not have ethical permission to apply sedation during scanning) but the techniques used to estimate growth can be readily transferred to such data. Using Jacobian determinant maps that represent growth on a per-voxel basis, we have generated growth estimates for white and grey matter for each individual and for the cohort as a whole. In the exemplar study of 25 ex-preterm infants, there was an increase of around 10–12% for grey matter and an increase in white matter growth of around 25–30%(see Fig. 13). Comparing tissue class growth estimates with estimates obtained from tissue segmentation shows excellent agreement on grey matter growth but higher variability in the estimates for white matter growth, suggesting a possible increased susceptibility to error, perhaps due to relatively smaller volume of white matter, changes in myelination and partial volume effects.

The volumes of each tissue at each timepoint, as shown in Fig. 11, illustrate the correspondences between baseline and follow-up volumes. Without making any assumptions about the best model for the growth (e.g. linear, nonlinear, etc.) these correspondences suggest that the development at this age follows what is described as a ‘parallel trajectory’ by Kraemer et al. (2000). Allometric studies of brain development (for example, see Kapellou et al., 2006; Zhang and Sejnowski, 2000) are made possible by these data, and the DBM approach has been successfully used for studies of more immature brains, and thus a combination of the DBM approach with automatic brain labelling holds the promise of a large scale neuroinformatic understanding of brain development during this period of rapid growth.

We have used intersubject registrations to generate average space atlases for the cohort at each timepoint. These atlases have taken the form of the average anatomy or average tissue class maps

Table 1
Growth factor estimates obtained by segmentation and registration

Growth factors	Grey matter	White matter
Segmentation	1.12 (0.030)	1.28 (0.049)
Registration	1.11 (0.035)	1.26 (0.046)

The segmentation estimates were obtained from the ratio of volumes of each tissue at each age and averaged across subjects. The registration estimates were obtained by integration of Jacobian determinants as described in Eq. (2). Standard deviations are shown in brackets.

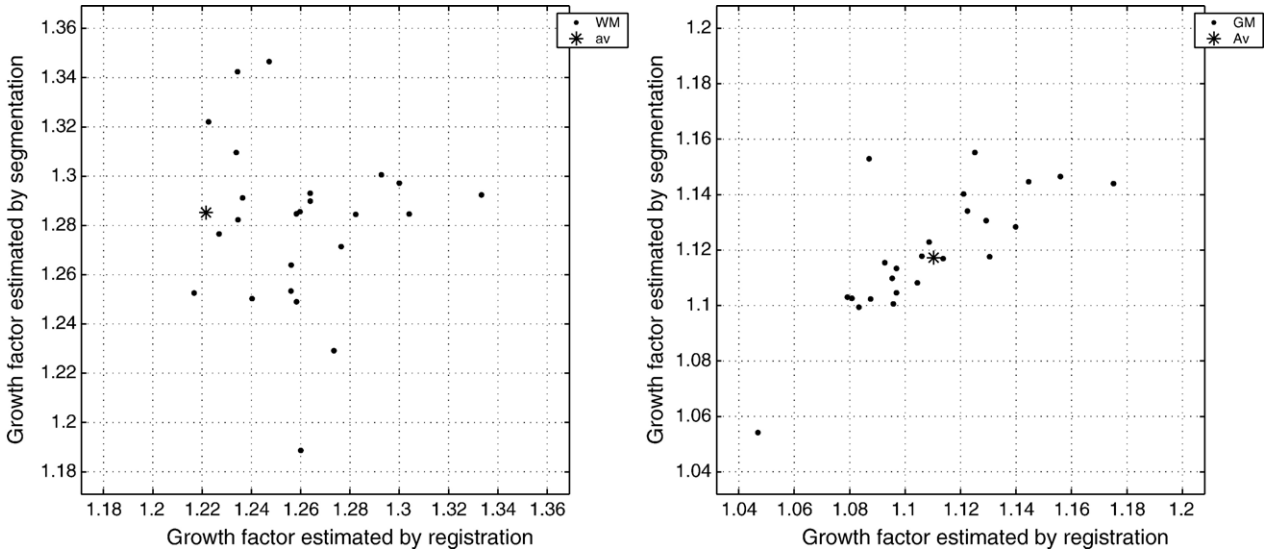

Fig. 13. Separate plots of growth factor estimates for WM and GM. Each diagram also indicates (with an asterisk) the growth factor obtained by using the tissue map atlases along with the growth map atlas.

at each timepoint and we have also estimated the average growth map for the baseline timepoint. In general, across the population, the pattern of change mainly represented by relatively higher growth within white matter, especially for the anterior white matter region (see Fig. 7) and a general contraction in the ventricular region which can be observed, for example, by comparing the one and two year images in Fig. 6.

A visual comparison of two average space atlases generated using two different reference subjects (Fig. 10) shows them to be in close agreement. This suggests that the bias towards the chosen reference has been significantly reduced. The approach used to create the atlases is similar to that used by Guimond et al. (2000) and Rueckert et al. (2003) who both showed that the atlases generated are reasonably robust to the choice of reference when the transformations being averaged are the local deformation fields. Our results indicate that this robustness remains when the averaged transformations incorporate the global affine component. It would be interesting, however, to investigate different approaches to the creation of the atlas, for example those presented in Wang et al. (2005), and assess their impact upon the resulting growth figures.

The growth factor estimates provided in this work have been given for tissue classes as defined by a tissue segmentation algorithm. The DBM approach, however, would allow growth factor estimates for other structures to be provided when used alongside other segmentation methods. We are currently working to extend to young children a structural segmentation method that we have previously applied to adult data (Heckemann et al., 2006a,b). When used in conjunction with the methods described in this paper, we should then be able to provide estimates of infant brain growth for more specific regions in the brain.

We have used the longitudinal transformations to estimate growth using the Jacobian determinants and given an illustration of the average longitudinal deformation field for the cohort. There are many other properties of the longitudinal deformation fields that can be extracted and subsequently used to answer questions about the patterns of development. For example, the curl or divergence of the fields can be calculated or estimates of the main modes of variation in the fields can be estimated (Rueckert et al., 2003). These options were beyond the scope of this work but should provide a very interesting area for future research.

We are not aware of other longitudinal studies estimating brain morphometry for children at these ages.

References

Alexa, M., 2002. Linear combination of transformations. ACM Trans. Graph. 21 (3), 380–387.

Aljabar, P., Bhatia, K., Hajnal, J., Boardman, J., Srinivasan, L., Rutherford, M., Dyet, L., Edwards, A., Rueckert, D., 2006. Analysis of growth in the developing brain using non-rigid registration. Proceedings of IEEE International Symposium on Biomedical Imaging (ISBI), Arlington, VA, April 2006, pp. 201–204.

Arsigny, V., Fillard, P., Pennec, X., Ayache, N., 2005. Fast and simple calculus on tensors in the log-Euclidean framework. Eighth Int. Conf. on Medical Image Computing and Computer-Assisted Intervention (MICCAI '05). Lecture Notes in Computer Science, vol. 3749, pp. 115–122.

Ashburner, J., Friston, K.J., 2000. Voxel-based morphometry—the methods. NeuroImage 11 (6), 805–821.

Avants, B., Gee, J., 2004. Shape averaging with diffeomorphic flows for atlas creation. ISBI, pp. 595–598.

Bhatia, K., Hajnal, J., Puri, B., Edwards, A., Rueckert, D., 2004. Consistent group wise non-rigid registration for atlas construction. Proceedings of IEEE International Symposium on Biomedical Imaging (ISBI), Arlington, VA, April, 2004, pp. 908–911.

Bhatia, K., Hajnal, J., Edwards, A., Rutherford, M., Rueckert, D., 2005. Group wise atlas construction for the identification of neuroanatomical changes associated with preterm birth. Proceedings International Society for Magnetic Resonance in Medicine (ISMRM), Miami, USA, p. 643.

Boardman, J.P., Counsell, S.J., Kapellou, O., Rueckert, D., Rutherford, M., Stark, J., Bhatia, K.K., Aljabar, P., Allsop, J., Hajnal, J.V., Edwards, D., 2005a. Neural systems affected by preterm birth. Proceedings International Society for Magnetic Resonance in Medicine (ISMRM), Miami, USA, p. 299.

Boardman, J., Counsell, S., Kapellou, O., Rueckert, D., Hajnal, J., Bhatia, K., Aljabar, P., Rutherford, M., Allsop, J., Edwards, A., 2005b. White matter abnormality is associated with volume reduction in deep grey nuclei following preterm birth. Pediatr. Res. 58 (2), 362–362.

Boardman, J., Counsell, S., Rueckert, D., Capellou, O., Bhatia, K., Aljabar,

P., Hajnal, J., Allsop, J., Rutherford, M., Edwards, A., 2006. Abnormal deep grey matter development following preterm birth detected using deformation based morphometry. NeuroImage 32 (1), 70–78.

Bossa, M.N., Olmos, S., 2006. Statistical model of similarity transformations: building a multi-object pose. Computer Vision and Pattern Recognition Workshop, p. 59.

Botting, N., Psychological and educational outcome of very low birth weight children at 12 years, PhD thesis, University of Liverpool (1997).

Chung, M.K., Worsley, K.J., Paus, T., Cherif, D.L.C.C., Giedd, J.N., Rapoport, J.L., Evans, A.C., 2001. A unified statistical approach to deformation-based morphometry. NeuroImage 14 (3), 595–606.

Craene, M.D., du Bois d'Aische, A., Macq, B., Warfield, S., 2004. Multi-subject registration for unbiased statistical atlas construction. Seventh Int. Conf. on Medical Image Computing and Computer-Assisted Intervention (MICCAI '04). Lecture Notes in Computer Science, vol. 3216, pp. 655–662.

Davatzikos, C., Vaillant, M., Resnick, S.M., Prince, J.L., Letovsky, S., Bryan, R.N., 1996. A computerized approach for morphological analysis of the corpus callosum. J. Comput. Assist. Tomogr. 20, 88–97.

Durston, S., Pol, H.H., Casey, B., Giedd, J., Buitelaar, J., van Engeland, H., 2001. Anatomical MRI of the developing human brain: what have we learned? J. Am. Acad. Child Adolesc. Psych. 40 (9), 1012–1020.

Gerig, G., Davis, B., Lorenzen, P., Xu, S., Jomier, M., Piven, J., Joshi, S., 2006. Computational anatomy to assess longitudinal trajectory of brain growth. Proceedings of the Third International Symposium on 3D Data Processing, Visualization, and Transmission (3DPVT), pp. 1041–1047.

Giedd, J.N., Snell, J.W., Lange, N., Rajapakse, J.C., Casey, B.J., Patricia, A.C.V., Kozuch, L., Vauss, Y.C., Hamburger, S.D., Kaysen, D., Rapoport, J.L., 1996. Quantitative magnetic resonance imaging of human brain development ages 4–18. Cereb. Cortex 6, 551–560.

Giedd, J.N., Jeffries, N.O., Castellanos, F.X., Liu, H., Zijdenbos, A., Paus, T., Evans, A.C., Rapoport, J.L., 1999. Brain development during childhood and adolescence: a longitudinal MRI study. Nat. Neurosci. 2 (10), 861–863.

Guimond, A., Meunier, J., Thirion, J.-P., 2000. Average brain models: a convergence study. Comput. Vis. Image Underst. 77, 192–210.

Heckemann, R.A., Hajnal, J.V., Aljabar, P., Rueckert, D., Hammers, A., 2006a. Automatic anatomical brain MRI segmentation combining label propagation and decision fusion. NeuroImage 33 (1), 115–126.

Heckemann, R., Hajnal, J., Aljabar, P., Rueckert, D., Hammers, A., 2006b. Multi classifier fusion in human brain MR segmentation: modelling convergence. Ninth Int. Conf. on Medical Image Computing and Computer-Assisted Intervention (MICCAI'06), vol. 4191, pp. 815–822.

Huppi, P.S., Warfield, S., Kikinis, R., Barnes, P.D., Zientara, G.P., Jolesz, F.A., Tsuji, M.K., Volpe, J.J., 1998. Quantitative magnetic resonance imaging of brain development in premature and mature newborns. Ann. Neurol. 43 (2), 224–235.

Kapellou, O., Counsell, S.J., Kennea, N., Dyet, L., Saeed, N., Stark, J., Maalouf, E., Duggan, P., Ajayi-Obe, M., Hajnal, J., Allsop, J.M., Boardman, J., Rutherford, M.A., Cowan, F., Edwards, A.D., 2006. Abnormal cortical development after premature birth shown by altered allometric scaling of brain growth. PLoS Med. 3 (8), e265.

Kraemer, H.C., Yesavage, J.A., Taylor, J.L., Kupfer, D., 2000. How can we learn about developmental processes from cross-sectional studies, or can we? Am. J. Psychiatry 157 (2), 163–171.

Leemput, K.V., Maes, F., Vandermeulen, D., Suetens, P., 1999. Automated model-based tissue classification of MR images of the brain. IEEE Trans. Med. Imag. 18 (10), 897–908.

Lorenzen, P., Davis, B., Gerig, G., Bullitt, E., Joshi, S., 2004. Multi-class posterior atlas formation via unbiased kullback-leibler template estimation. Seventh Int. Conf. on Medical Image Computing and Computer-Assisted Intervention (MICCAI'04). Lecture Notes in Computer Science, vol. 3216, pp. 95–102.

Lorenzen, P., Davis, B., Joshi, S., 2005. Unbiased atlas formation via large deformations metric mapping. Eighth Int. Conf. on Medical Image Computing and Computer-Assisted Intervention (MICCAI '05). LNCS, vol. 3750, pp. 411–417.

Marlow, N., Wolke, D., Bracewell, M., Samara, M., 2005. Neurologic and developmental disability at six years of age after extremely preterm birth. N. Engl. J. Med. 352 (1), 9–19.

Matsuzawa, J., Matsui, M., Konishi, T., Noguchi, K., Gur, R.C., Bilker, W., Miyawaki, T., 2001. Age-related volumetric changes of brain gray and white matter in healthy infants and children. Cereb. Cortex 11 (4), 335–342.

Murgasova, M., Dyet, L.E., Edwards, A.D., Rutherford, M., Hajnal, J.V., Rueckert, D., 2006. Segmentation of brain MRI in young children. Ninth Int. Conf. on Medical Image Computing and Computer-Assisted Intervention (MICCAI '06). Lecture Notes in Computer Science, vol. 4190, pp. 687–694.

Nishida, M., Makris, N., Kennedy, D.N., Vangel, M., Fischl, B., Krishnamoorthy, K.S., Caviness, V.S., Grant, P.E., 2006. Detailed semi automated MRI based morphometry of the neonatal brain: preliminary results. NeuroImage 32 (3), 1041–1049.

Rao, A., Chandrashekara, R., Sanchez-Ortiz, G., Mohiaddin, R., Aljabar, P., Hajnal, J., Puri, B., Rueckert, D., 2004. Spatial transformation of motion and deformation fields using non-rigid registration. IEEE Trans. Med. Imag. 23 (9), 1065–1076.

Rao, A., Cootes, T., Rueckert, D., 2006. Hierarchical statistical shape analysis and prediction of sub-cortical brain structures. Computer Vision and Pattern Recognition Workshop, 2006 Conference on, p. 75–75.

Rueckert, D., Sonoda, L., Hayes, C., Hill, D., Leach, M., Hawkes, D., 1999. Non-rigid registration using free-form deformations: application to breast MR images. IEEE Trans. Med. Imag. 18 (8), 712–721.

Rueckert, D., Frangi, A.F., Schnabel, J.A., 2003. Automatic construction of 3D statistical deformation models of the brain using non-rigid registration. IEEE Trans. Med. Imag. 22 (8), 1014–1025.

Schnabel, J.A., Rueckert, D., Quist, M., Blackall, J.M., Castellano-Smith, A.D., Hartkens, T., Penney, G.P., Hall, W.A., Liu, H., Truwit, C.L., Gerritsen, F.A., Hill, D.L.G., Hawkes, D.J., 2001. A generic framework for non-rigid registration based on non-uniform multi-level free-form deformations. In: Niessen, W.J., Viergever, M.A. (Eds.), Fourth Int. Conf. on Medical Image Computing and Computer-Assisted Intervention (MICCAI '01). Lecture Notes in Computer Science, vol. 2208, pp. 573–581.

Sederberg, T.W., Parry, S.R., 1986. Free-form deformation of solid geometric models. In: Robinson, K. (Ed.), Proceedings of the 13th Annual Conference on Computer Graphics and Interactive Techniques (SIGGRAPH), Dallas, USA, August, 1986, pp. 151–160.

Sled, J.G., Zijdenbos, A.P., Evans, A.C., 1998. A non-parametric method for automatic correction of intensity non-uniformity in MRI data. IEEE Trans. Med. Imag. 17 (1), 87–97.

Smith, S., 2002. Fast robust automated brain extraction. Hum. Brain Mapp. 17 (3), 143–155.

Sowell, E.R., Thompson, P.M., Leonard, C.M., Welcome, S.E., Kan, E., Toga, A.W., 2004. Longitudinal mapping of cortical thickness and brain growth in normal children. J. Neurosci. 24 (38), 8223–8231.

Studholme, C., Hill, D.L.G., Hawkes, D.J., 1998. An overlap in variant entropy measure of3D medical image alignment. Pattern Recogn. 32 (1), 71–86.

Thompson, P.M., Giedd, J.N., Woods, R.P., MacDonald, D., Evans, A.C., Toga, A.W., 2000. Growth patterns in the developing brain detected by continuum mechanical tensor maps. Nature 404, 190–193.

Unser, M., 1999. Splines: a perfect fit for signal and image processing. IEEE Signal Process. Mag. 22–38.

Wahba, G. (Ed.), 1990. Spline Models for Observational Data. Society for Industrial and Applied Mathematics.

Wang, Q., Seghers, D., D'Agostino, E., Maes, F., Vandermeulen, D., Suetens, P., Hammers, A., 2005. Construction and validation of mean shape atlas templates for atlas-based brain image segmentation. Information Processing in Medical Imaging: Proc. 19th International Conference(IPMI'01), pp. 689–700.

Zhang, K., Sejnowski, T.J., 2000. A universal scaling law between gray matter and white matter of cerebral cortex. Proc. Natl. Acad. Sci. U. S. A. 97, 5621–5626.